JGR Oceans

RESEARCH ARTICLE
10.1029/2021JC017845

Decadal Variations in Radiocarbon in Dissolved Inorganic Carbon (DIC) Along a Transect in the Western North Pacific Ocean

Tiantian Ge[1], Chunle Luo[1], Peng Ren[1,2], Hongmei Zhang[1], Zhaohui Chen[3], Shuwen Sun[2], Liping Xu[2], and Xuchen Wang[1,2]

[1]Key Laboratory of Marine Chemistry Theory and Technology, Frontiers Science Center for Deep Ocean Multispheres and Earth System, Ocean University of China, Qingdao, China, [2]Center for Isotope Geochemistry and Geochronology, Qingdao National Laboratory for Marine Science and Technology, Qingdao, China, [3]Key Laboratory of Physical Oceanography, Frontiers Science Center for Deep Ocean Multispheres and Earth System, Ocean University of China, Qingdao, China

Key Points:

- Strong bomb ^{14}C signals are well mixed into the upper 200–500 m water depth through air-sea exchange long a transect in the western NP Ocean
- Distribution of radiocarbon in DIC in the Kuroshio Extension region was influenced strongly by Oyashio Currents carrying low $\Delta^{14}C$ values
- Bomb ^{14}C penetration signal in the NP has been reduced and diluted by deep waters carrying depleted ^{14}C-DIC over the last 30 years

Supporting Information:

Supporting Information may be found in the online version of this article.

Correspondence to:

X. Wang,
xuchenwang@ouc.edu.cn

Citation:

Ge, T., Luo, C., Ren, P., Zhang, H., Chen, Z., Sun, S., et al. (2022). Decadal variations in radiocarbon in dissolved inorganic carbon (DIC) along a transect in the western North Pacific Ocean. *Journal of Geophysical Research: Oceans*, *127*, e2021JC017845. https://doi.org/10.1029/2021JC017845

Received 2 AUG 2021
Accepted 12 JAN 2022

Author Contributions:

Conceptualization: Xuchen Wang
Data curation: Chunle Luo, Hongmei Zhang, Zhaohui Chen, Shuwen Sun, Liping Xu
Formal analysis: Tiantian Ge, Chunle Luo, Hongmei Zhang, Shuwen Sun, Liping Xu
Funding acquisition: Zhaohui Chen, Xuchen Wang
Investigation: Tiantian Ge, Chunle Luo, Peng Ren, Zhaohui Chen, Xuchen Wang
Methodology: Tiantian Ge, Chunle Luo, Peng Ren, Hongmei Zhang, Liping Xu, Xuchen Wang
Project Administration: Zhaohui Chen
Resources: Xuchen Wang
Software: Hongmei Zhang, Shuwen Sun, Liping Xu
Supervision: Xuchen Wang

Abstract We report results for the concentrations and radiocarbon (^{14}C) compositions of dissolved inorganic carbon (DIC) in water samples collected from a north-south transect in the western North Pacific (NP) Ocean in November 2019 and compare our results with values previously reported for similar transects during the WOCE and CLIVAR projects decades ago. We show that the strong bomb ^{14}C penetration signal in the upper waters has gradually been reduced and diluted by deep water depleted in ^{14}C-DIC over the last 30 years. The rate of decrease in $\Delta^{14}C$-DIC values in surface waters was greater from 2005 to 2019 than from 1993 to 2005, and the rates of decrease from 2005 to 2019 were fastest (5.4–7.0‰ yr^{-1}) between 25° and 32°N and slowest (2.1–2.8‰ yr^{-1}) between 13°N and 16°N. The downwelling of the water mass could have accelerated the transport of bomb ^{14}C in the NP subtropical gyre (25°–32°N). The different decadal changes in $\Delta^{14}C$-DIC in the North Pacific Intermediate Water (NPIW) from north to south prove that bomb ^{14}C is transported southward to the southwestern NP and that the bomb ^{14}C peak likely penetrates the ocean interior gradually. Changes in isopycnic circulation and advection diffusion in deep waters might have resulted in shifts in the baseline $\Delta^{14}C$-DIC signature.

Plain Language Summary Dissolved inorganic carbon (DIC) in the ocean is the largest pool of exchangeable carbon in the world and plays dominant roles in the global carbon cycle. The North Pacific (NP) Ocean is an important, highly dynamic region that accounts for ~25% of the annual CO_2 global ocean sink from the atmosphere. To study the sources and cycling of DIC in the western NP, we measured radiocarbon, a powerful tracer, in DIC in water samples collected from 26 stations along a transect in the western NP in November 2019. We compared our results with data reported for similar transects in the NP sampled during the World Ocean Circulation Experiment (WOCE) and the Climate Variation and Predictability Program (CLIVAR) decades ago. The large data set enables us to evaluate the decadal changes in DIC concentrations and radiocarbon compositions in the western NP and to gain fresh knowledge about the carbon cycles linked to water circulation and mixing processes in the western NP.

1. Introduction

The oceans represent a significant sink for atmospheric CO_2, acting as the largest pool of exchangeable carbon in the world. Globally, approximately 39,000 GtC of total carbon is stored in the ocean, up to 95% of which is in the form of dissolved inorganic carbon (DIC; Key et al., 2004; Schuur et al., 2016). Each year, approximately 30%–40% of anthropogenically produced CO_2 is absorbed by the ocean through air-sea exchange and dissolved as DIC in the ocean (Gruber et al., 2009; Lemke et al., 2007). The variability in DIC in the ocean is controlled not only by air-sea exchange (Tsunogai, 2000; Winn et al., 1998) but also by changes in ocean circulation and biological activities (Gruber, 2011; Tsurushima et al., 2002; Wakita et al., 2010). The distribution and cycling of DIC in the ocean therefore play crucial roles in the global carbon cycle and in climate change (Key et al., 2004; Valsala et al., 2012; Yasunaka et al., 2014).

Radiocarbon (^{14}C) natural abundances have been used in studies of marine carbon cycling to determine the sources, residence times, transformations, and interactions of both organic and inorganic carbon reservoirs (Bauer et al., 1992; Druffel et al., 1992; Key et al., 1996; McNichol et al., 2000; Stuiver et al., 1996; Williams &

Validation: Tiantian Ge, Chunle Luo, Peng Ren, Hongmei Zhang, Xuchen Wang
Writing – original draft: Tiantian Ge
Writing – review & editing: Xuchen Wang

Druffel, 1987). The first global survey of oceanic ^{14}C in DIC in the Pacific Ocean was conducted during the Geochemical Ocean Sections Study (GEOSECS) in the 1970s, and the second survey was conducted during the World Ocean Circulation Experiment (WOCE) in the 1990s; monitoring was subsequently continued during the Climate Variation and Predictability Program (CLIVAR) in the 2000s. These successful international cooperative research efforts have collected many DIC samples from the global ocean and have generated the largest current database of information on ^{14}C-DIC in the world ocean (Broecker et al., 1995; Key et al., 1996; Kumamoto et al., 2013; McNichol et al., 2000; Sarnthein et al., 2013; Stuiver et al., 1983, 1996). The radiocarbon results obtained in these previous joint international studies have provided great insight that enhances our understanding of the oceanic carbon cycle and of ocean circulation processes linked to climate variability (Broecker et al., 1995; Druffel et al., 2008; Key et al., 2004; Kumamoto et al., 2013; Sarnthein et al., 2013; Stuiver et al., 1983).

Early radiocarbon measurements of DIC in seawater revealed transit times of hundreds to thousands of years for the deep-water masses in the world's oceans (Bien et al., 1963; Broecker et al., 1960; Stuiver et al., 1983). Due to the movement of water masses, the DIC ages in the deep North Pacific (NP) Ocean have been found to be ~2,000 ^{14}C years BP (before present), much older than the North Atlantic Ocean DIC ^{14}C ages (~650 years BP; Druffel et al., 2008). The penetration of bomb ^{14}C derived from nuclear weapons tests in the late 1950s and early 1960s has provided information about air-sea gas exchange and thermocline circulation in the ocean (Druffel et al., 2008; Key et al., 2004; Kumamoto et al., 2013). The bomb ^{14}C in surface water enters the atmosphere through CO_2 gas exchange and penetrates the ocean interior by water advection and diffusion. High surface ^{14}C values in DIC due to exchange with atmospheric CO_2 have been mixed to a depth of at least 1000 m in most areas of the world's oceans (Druffel et al., 2008; Key et al., 2004; Kumamoto et al., 2013).

The Pacific Ocean is the largest and deepest ocean in the world. The NP Ocean is an important, highly dynamic region that accounts for ~25% of the annual CO_2 global ocean sink from the atmosphere (Takahashi et al., 2009), and most of the carbon absorption of this region occurs across a swath of the basin (30°–45°N) at the junction of the subtropical gyre and the subarctic region. The Kuroshio and Oyashio Currents, as well as the Kuroshio Extension (KE) formed by the mixture of these two currents, are the most important currents within the complex circulation system in the northwest NP Ocean. The KE is a highly dynamic region where the Kuroshio and Oyashio Currents meet and influence the hydrology and chemical properties of the resulting water mass (Tsunogai et al., 1995; Tsurushima et al., 2002). The KE region has been reported to be the strongest sink of atmospheric CO_2 in the NP Ocean (Takahashi et al., 2009).

During recent decades, several studies have been conducted using ^{14}C as a tracer to assess the carbon cycle, the regional climate and the spatial and temporal variability of circulation processes in the NP Ocean. The decadal changes in bomb-produced ^{14}C measured in DIC in the NP from the 1990s to the 2000s showed that bomb ^{14}C was transported from the subarctic zone to the subtropical area of the NP (Kumamoto et al., 2002, 2013). Moreover, the turnover time of thermocline circulation in the northwestern subtropical region is faster than that in the southern subtropical region due to the transport of North Pacific Intermediate Water (NPIW; Kumamoto et al., 2013). Tsunogai et al. (1995) found that the temporal change in radiocarbon at the lower isopycnal surface of the NPIW in the western NP is smaller than would be expected based on the DIC increase, indicating active isopycnal mixing (Tsunogai et al., 1995). DIC and $\Delta^{14}C$ values, which are relatively conservative tracers, have been used to research water mass movement and mixing in the NP Ocean (Beaupre & Aluwihare, 2010; Ding et al., 2018; Ge et al., 2016). In our previous study, we found that the large variability in $\Delta^{14}C$ values in the upper 500-m water layer in the KE region was related mainly to the Oyashio Current, which carries water with high DIC concentrations and low subarctic intermediate water with low $\Delta^{14}C$ values, and the Kuroshio Current, which carries water with relatively lower DIC $\Delta^{14}C$ values to the region (Ding et al., 2018); these observations indicated that different water masses and circulation mixing play important roles in controlling the distribution of both DIC and $\Delta^{14}C$.

In this paper, we present new $\Delta^{14}C$-DIC results for water samples collected in 2019 from a north-south transect, P1 (13°–40°N, 150°E), in the northwestern NP Ocean (Figure 1). This is a transect close to those that were investigated during repeated hydrographic cruises associated with the WOCE study (line P10, ~149.3°E) in 1993 (Key, 1996; Key et al., 2004; McNichol et al., 2000; Stuiver et al., 1996) and during the CLIVAR cruise (line P10N, ~149.3°E) in 2005 (Kumamoto et al., 2013). Comparison of the data obtained during the three cruises conducted along these close transects in the western NP in 1993, 2005, and 2019 enables us to evaluate the decadal changes in DIC concentrations and ^{14}C compositions in the western NP and to gain knowledge about the carbon cycles linked to water circulation and mixing processes in the western NP.

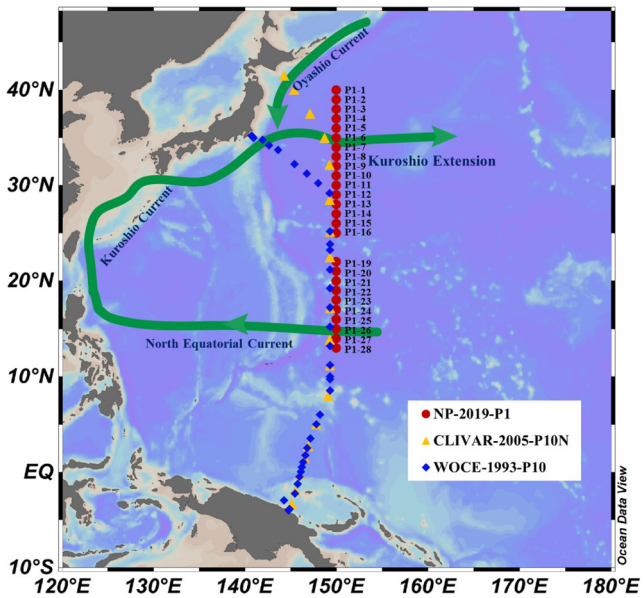

Figure 1. Map of the study region plotted using Ocean Data View (ODV, Schlitzer, 2015) and the sampling transect stations of line P1 (red dots) in the northwestern North Pacific for which data were collected in November 2019. The sampling stations in this region that were used in this paper for comparison data are also shown: WOCE line P10 from 1993 (blue diamonds) and CLIVAR line P10N from 2005 (yellow triangles).

2. Methods

2.1. Study Region

The study area lies in the western NP Ocean (Figure 1), where wind-driven currents are the most dominant characteristics (Hu et al., 2015; Ma et al., 2016). The Kuroshio and Oyashio Currents are the western boundary currents in the wind-driven, subtropical and subarctic circulations of the NP, and they greatly influence the climate, ecosystems, and carbon cycle in the western NP and adjacent waters. The Kuroshio is characterized by saline, warm, and oligotrophic waters of the subtropical gyre; it transports waters from the northern Philippines, the area east of Taiwan Island, and along the continental slope of the East China Sea (ECS) and the southern coast of the Japanese Archipelago and then flows eastward to the open basin of the NP, where it is renamed the KE Current (Hu et al., 2015; Takahashi et al., 2009). The Oyashio Current, in comparison, is characterized by cold water, low salinity, and high nutrient levels and is formed by a mixture of upwelled waters from the western subarctic gyre and waters of the Sea of Okhotsk. At approximately 34°–37°N, the Oyashio front meets the KE Current and forms the Kuroshio-Oyashio interfrontal zone, where the subarctic water mass mixes with the relatively warm and saline KE water, and the mixed waters then flow eastward (Hu et al., 2015; Qiu & Chen, 2011; Rogachev et al., 2000; Yasuda, 2004; Yasuda et al., 1996). The Kuroshio-Oyashio interfrontal zone is the most dynamic region in the NP with respect to sea surface height, eddy activity, and sea surface temperature (SST) and is the region in which the largest heat loss from the ocean to the atmosphere occurs (Qiu & Chen, 2011).

NPIW circulation is generated around the Okhotsk Sea due to tidal-induced diapycnal mixing and dense shelf water formation accompanied by sea ice formation and is transported through the south-flowing Oyashio along the western boundary from the subarctic region to the Kuroshio-Oyashio interfrontal zone (Yasuda, 2004). In this area, cold and fresh subarctic (Oyashio) water intrudes into the intermediate layer of warm and salty subtropical (Kuroshio) water. The mixture of these two end members forms a new NPIW that is characterized by a vertical salinity minimum at a potential density of 26.3–27.2σ_θ (Talley, 1993; Tally & Lynne, 1997; Tsunogai et al., 1993; Yasuda et al., 1996). The NPIW is important with respect to anthropogenic carbon dioxide because the subarctic water mass that is richer in anthropogenic carbon dioxide is transported to the south and widely distributed in the intermediate layer of the NP subtropical gyre (Qiu & Chen, 2011; Tsunogai et al., 1993; Yasuda et al., 1996).

The deep ocean occupies a major part of the marine system. The deep circulation of the world ocean plays a large role in the carbon cycle by transporting greenhouse effect gases. Changes in the resident water masses, in their rates of ventilation and in the relative rate of regeneration of biogenic carbon could influence the magnitude of carbon storage. The deepest part of the global overturning circulation is Antarctic bottom water (AABW). As the near-bottom water mass enters the NP from the south, it gains buoyancy via vertical mixing; it thus rises to the middle of the water column and returns south as Pacific deep water (Macdonald et al., 2009; Talley, 2013).

2.2. Sample Collection

The water samples used in DIC analyses were collected at 26 stations along transect P1 (13°–40°N, 150°E) in the western NP during a cruise on *R/V* Dongfanghong 3 in November 2019 (Figure 1). General information about the sampling stations is provided in Table 1. Seawater samples were collected along the entire water depth at 7 stations and from only the upper 2,000-m layer at 19 stations. Water was collected using 12-L Niskin bottles attached to a rosette sampler with conductivity, temperature, and depth sensors that recorded the temperature and salinity profiles. For DIC water collection, we used the protocol described by McNichol and Jones (1991). Water was collected (after overflowing ~100 mL) in prebaked 100-mL glass bottles with fine ground-glass stoppers using precleaned silicone tubing connected directly to the Niskin bottle. Each collected sample was immediately treated with 50 μL of saturated $HgCl_2$ solution. The bottles were then capped tightly using a grease-coated,

Table 1
Description of the Sampling Site in Western North Pacific Ocean

Station no.	Latitude (°N)	Longitude (°E)	Bottom depth (m)	Sample depth
P1-1	40	150	5,678	Full water depth
P1-2	39	150	5,370	2,000 m
P1-3	38	150	6,066	2,000 m
P1-4	37	150	5,825	2,000 m
P1-5	36	150	2,979	Full water depth
P1-6	35	150	6,081	2,000 m
P1-7	34	150	6,015	2,000 m
P1-8	33	150	5,972	2,000 m
P1-9	32	150	5,834	Full water depth
P1-10	31	150	5,998	2,000 m
P1-11	30	150	5,931	2,000 m
P1-12	29	150	5,957	2,000 m
P1-13	28	150	6,026	Full water depth
P1-14	27	150	5,836	2,000 m
P1-15	26	150	5,871	2,000 m
P1-16	25	150	5,749	2,000 m
P1-19	22	150	4,826	2,000 m
P1-20	21	150	5,742	2,000 m
P1-21	20	150	2,824	Full water depth
P1-22	19	150	5,467	2,000 m
P1-23	18	150	5,102	2,000 m
P1-24	17	150	1,448	2,000 m
P1-25	16	150	5,661	Full water depth
P1-26	15	150	2,828	2,000 m
P1-27	14	150	6,028	2,000 m
P1-28	13	150	6,028	2,000 m

ground-glass stopper secured with rubber bands to create a gas-tight seal to prevent exchange of CO_2 with the atmosphere. All DIC samples were kept in the dark at room temperature and analyzed in the laboratory within one month after collection.

2.3. Analysis of DIC Concentrations

DIC concentrations were analyzed using the total inorganic carbon mode of a Shimadzu TOC-L analyzer equipped with an ASI-V autosampler. Reagent-grade sodium carbonate and sodium bicarbonate dissolved in high-purity Milli-Q water were used as the DIC standard. DIC concentrations were calibrated using a six-point standard calibration curve. The instrument blank and the DIC values were checked against DIC reference materials (certified reference materials (CRMs, Batch No. 177) supplied by Dr. A. Dickson at Scripps Institution of Oceanography). The total blanks associated with DIC measurements were <3.0 μM, a value that is approximately <0.15% of the seawater DIC concentrations measured, and the analytical precision was <2% based on triplicate injections (Ding, et al., 2018).

2.4. DIC Isotopic Measurements

DIC was extracted from water samples as gaseous CO_2, and the extracted CO_2 was purified on a vacuum system using our modified method (Ge et al., 2016) based on McNichol et al. (1994). Briefly, in an N_2-filled glove box, a 50-mL water sample was injected into a pre-evacuated 100-mL borosilicate glass bottle with ground-glass joint stripping probes. After the injection of 1.0 mL of 85% H_3PO_4 using a glass syringe and a stainless-steel needle, the glass bottle containing the acidified water sample was placed in a hot-water bath (70°C) for 30 min, during which time it was shaken by hand several times. Under these conditions, all forms of DIC (carbonate, bicarbonate, and CO_2) in the water were converted to CO_2 in the glass bottle. After cooling, the glass bottle was connected to the vacuum line, and the CO_2 was collected cryogenically and quantified manometrically. The purified CO_2 was flame-sealed in a 6 mm-OD glass tube for isotope analysis. The efficiency of extraction of DIC with this method was >96% (Ge et al., 2016).

$\Delta^{14}C$ measurement was performed at the Center for Isotope Geochemistry and Geochronology (CIGG) of Qingdao National Laboratory for Marine Science and Technology (QNLM) in Qingdao, China. The purified CO_2 was graphitized using the sealed tube zinc reduction method (Walker & Xu, 2019; Xu et al., 2007), and ^{14}C was measured by accelerator mass spectrometry (AMS, NEC 0.5 MV Model 1.5SDH-1 Pelletron Accelerator XCAMS). The errors in DIC $\Delta^{14}C$ measurements based on duplicate sample analyses were ±3–4‰. Radiocarbon abundance was measured as fraction modern (FM) based on the standard reference material (NIST 4990C Oxalic Acid-II), and $\Delta^{14}C$ value and conventional ^{14}C age (year before present) were then calculated based on Stuiver and Polach (1977) and reported. When $\delta^{14}C$ values are ≥0‰, the ^{14}C ages are defined as modern.

3. Results

3.1. Hydrography

The water temperature, salinity, DIC concentrations and isotopic values measured at the sample stations are summarized in Table S1 in Supporting Information S1. The depth profiles and the latitudinal distributions of water temperature, salinity, and density for stations along the P1 transect are plotted in Figure 2. The water temperature was highest in the surface layer and higher at low latitudes than at high latitudes (Figures 2a and 2b). Sta P1-1 (40.04°N, 149.89°E) had the lowest water temperature (14.5°C), and Sta P1-28 (13.00°N, 149.99°E) had the

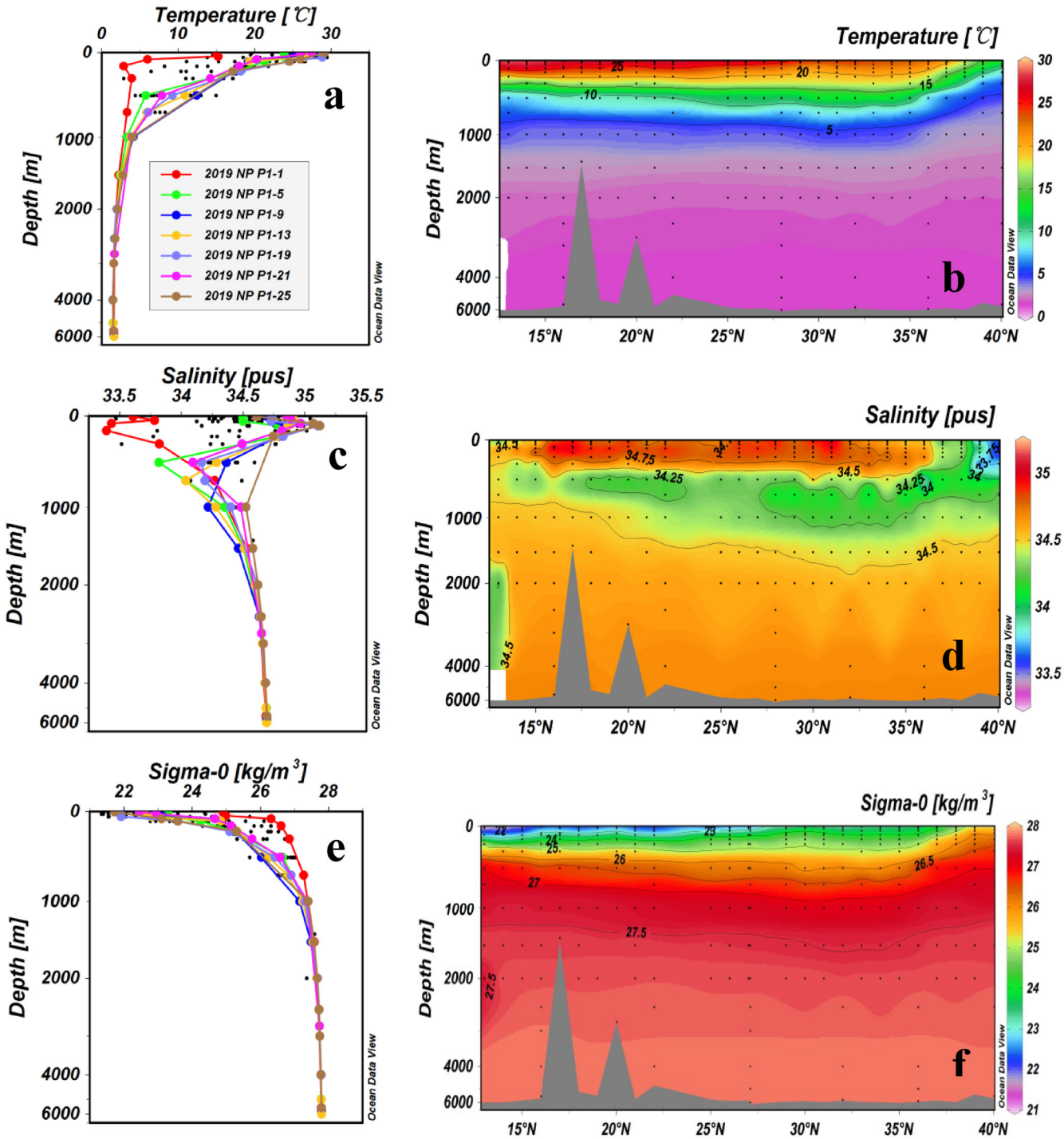

Figure 2. Depth profiles and latitudinal distributions of water temperature (a, b), salinity (c, d), and density (e, f) for stations along the P1 transect in the western NP in November 2019 using ODV. The density data were calculated by ODV (Schlitzer, 2015). The data for the 2,000-m sampling station are shown as black dots in the depth profiles.

highest water temperature (29.4°C) in the surface layer (5 m; Figure 2b and Table S1 in Supporting Information S1). The largest differences in the water temperature profiles appeared above a depth of 1,000 m (Figures 2a and 2b), showing that the water temperatures at the high-latitude stations (P1-1, P1-2, P1-3, P1-4, and P1-5; 36°–40°N) were obviously lower than those at the other stations, with water temperature generally decreasing unevenly with depth at all stations. Except at Stas P1-1 and P1-2, the water temperature decreased rapidly from

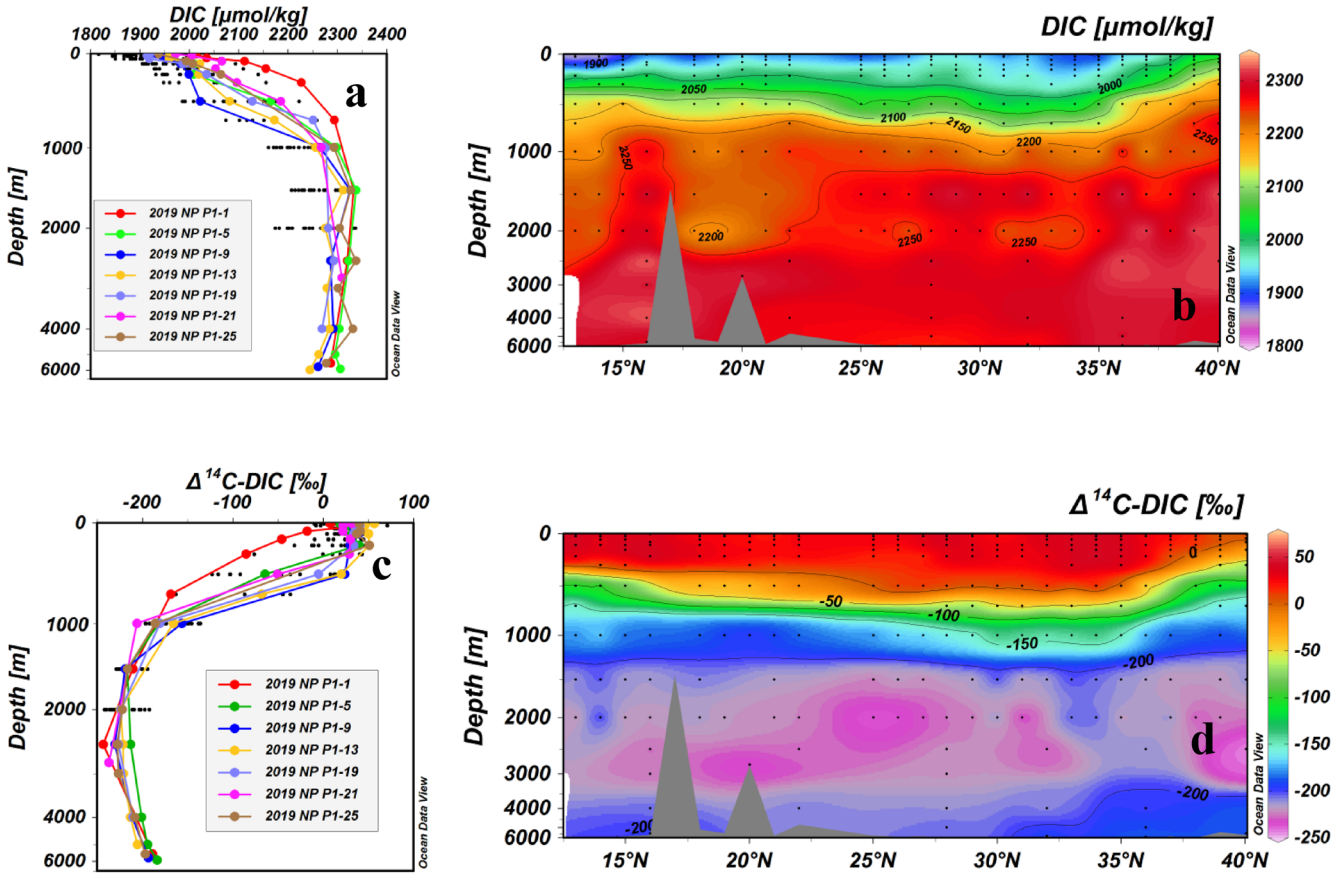

Figure 3. Depth profiles and latitudinal distributions of the DIC concentrations (a, b) and values of Δ^{14}C-DIC (c, d) measured for the stations along the P1 transect in the northwestern NP in November 2019 using ODV. The data for the 2,000-m sampling depths are shown as black dots in the depth profiles.

the surface down to 1,500 m (<3°C); it then remained constant below 1,500 m at density levels of $\sigma_0 \geq 27.5$ (Figures 2a and 2b). At Stas P1-1 and P1-2, which are located at high latitudes, the water temperature decreased rapidly to ~3°C in the upper layer (>155 m and >300 m, respectively); it then decreased to values similar to those measured at the other stations down to 1,500 m (Figures 2a and 2b).

The largest variations in water salinity profiles were also seen in the upper 1,000 m (Figures 2c and 2d). Salinities in the upper 500 m at stations at high latitudes (P1-1, P1-2, P1-3, and P1-4) were obviously lower than those at the other stations (Figure 2d). Sta P1-2 had the lowest salinity (33.463), and Sta P1-10 had the highest salinity (35.044) in the surface layer. The salinity increased unevenly with depth in the upper water (>155 m), decreased to the minimum by 500–750 m (~27σ_0), and then increased at greater depths before remaining constant (>34.5, $\sigma_0 \geq 27.5$) below 1,500 m between 13 and 38°N (Figures 2c and 2d). The water salinity profiles for stations P1-1 and P1-2 increased in the upper 50 m, decreased with depth to ~200 m, and then increased to values similar to those observed at the other stations at 2,500 m (Figure 2c). The water density in the P1 transect in the western NP was consistent with the salinity, showing dense water in the high north latitudes and low-density water at the surface in the low latitudes (<25°N; Figure 2f). Water density was quite constant (>34.5, $\sigma_0 \geq 27.5$) below 1,500 m depth overall (Figures 2e and 2f).

3.2. Concentrations and Distributions of DIC

Depth profiles and latitudinal distributions of the DIC concentrations for all stations along the P1 transect are shown in Figure 3. The DIC concentrations ranged from 1,816 to 2,354 μmol/kg; they were lower in the surface water (5 m; 1,816–2,014 μmol/kg) and increased rapidly with depth (Figures 3a and 3b). Laterally, large concentration variations are seen in the upper 1,000 m depth across the P1 transect (Figure 3b). In comparison with

the other stations, Sta P1-1 in the KE region had the highest DIC concentrations (2,014–2,333 μmol/kg) from 0 to 2,000 m depth. The highest DIC (2,014 μmol/kg) and the lowest DIC (1,816 μmol/kg) values in the surface water (5 m) were measured at Stas P1-1 and P1-27, respectively. Although the DIC profiles exhibited some variation among the stations, in general, the concentrations of DIC showed minimum values in the upper 50 m, increased from the surface down to ∼1,000–1,500 m, and then remained relatively constant or decreased slightly (Figures 3a and 3b).

3.3. Isotopic Composition of DIC

The $\Delta^{14}C$ values of the DIC samples varied from 57‰ to −227‰, and the $\Delta^{14}C$ depth profiles showed a trend opposite that of the DIC concentrations; $\Delta^{14}C$ values were high in the surface water and decreased with depth (Table S1 in Supporting Information S1, Figures 3c and 3d). The values of $\Delta^{14}C$ in the surface water (5–55 m) ranged from −10 to 57‰, and the $\Delta^{14}C$ values in the KE region (Sta P1-1 to P1-5) were generally lower than those at other stations; a negative value (−10‰) was even observed in the surface water at Sta P1-2 (Figure 3d). The depth profiles of $\Delta^{14}C$ showed that Sta P1-1 exhibited the minimum values in the waters above 1,000 m (Figures 3c and 3d). The $\Delta^{14}C$ values for almost all stations were high and modern ($\Delta^{14}C \geq 0$‰) above a certain depth (105–500 m for different stations) and decreased with depth, showing large variations in the upper 250–1,000 m. The lowest values were observed between depths of 1,500 and 3,000 m at all stations; they ranged from −243‰ at 40°N (2,500 m, Sta P1-1) to −207‰ at 14°N (1,500 m, Sta P1-27). The $\Delta^{14}C$ values increased slightly in the bottom waters (3,000–6,000 m; Figure 3c). The latitudinal distribution clearly reveals high values in the upper layer and low values of the $\Delta^{14}C$ layer present in the deep waters of the western NP (Figure 3d).

4. Discussion

4.1. DIC Isotopic Distributions in Water Masses of the Upper Ocean

The $\Delta^{14}C$ values measured in seawater DIC provide useful information about the movements of water masses and the penetration of anthropogenic CO_2 into the ocean (Druffel et al., 2008; Key et al., 2002; McNichol et al., 2000). The goal of our research was to compare our results with the WOCE data measured in 1993 (P10 line, ∼149.3°E) and the CLIVAR data from 2005 (P10N line, ∼149.3°E) so as to examine the decadal changes in water mass $\Delta^{14}C$-DIC in the western NP over the last three decades. The 1993 and 2005 data we used for comparison were extracted from the GLOPAD data set (https://www.glodap.info/), and the data have been discussed in previous studies (Key, 1996; Key et al., 2004; Kumamoto et al., 2013; McNichol et al., 2000; Stuiver et al., 1996).

Local water circulation, vertical mixing processes and mesoscale eddies in the thermocline circulation influence the variability in both DIC concentrations and isotopic values in the western NP (Broecker et al., 1985, 1995; Ding et al., 2018; Kumamoto et al., 2013). The temperatures, salinities, DIC concentrations and isotopic distributions measured at stations along transect P1 (Figure 3) indicate the mixed influence of air-sea exchange, ocean circulation and biological activities on the thermocline. The plots of water temperature versus salinity (T-S) clearly show that the concentrations of DIC and the $\Delta^{14}C$ values (shown as different colored points) are associated with potential density anomalies among water masses with different densities at the stations in the sampled region (Figure 4). The T-S diagrams also show that the values of $\Delta^{14}C$ decrease to relatively low levels (<−200‰) and the concentrations of DIC increase to relatively high levels (>2,200 μmol/kg) at water densities $\sigma_0 \geq 27.5$ for samples at all stations (Figure 4).

The $\Delta^{14}C$ values in the surface waters (5–200 m) measured during our cruise ranged from −10 to 57‰, with an average value of ∼30‰, similar to the $\Delta^{14}C$ values in the atmospheric CO_2 of the Northern Hemisphere (Gao et al., 2019; Zigah et al., 2017). The modern $\Delta^{14}C$ values in the upper 500 m of the water column indicate that bomb $\Delta^{14}C$ signals have mixed and diffused into the upper ocean through air-sea exchange. Studies that distinguish between natural radiocarbon and radiocarbon derived from nuclear weapon testing have shown that bomb ^{14}C has penetrated to a depth of at least 1,500 m in the NP (Kaizer et al., 2020; Key et al., 2002; Kumamoto et al., 2013). According to Broecker et al. (1995), the concentration of silicate can be used as a proxy for natural radiocarbon $\Delta^{14}C_{nat}$ (‰, $\Delta^{14}C_{nat} = -70 - [SiO_2]$), and the bomb-produced radiocarbon $\Delta^{14}C_{bomb}$ (‰) can be evaluated by subtracting $\Delta^{14}C_{nat}$ from the measured $\Delta^{14}C$ values ($\Delta^{14}C_{bomb} = \Delta^{14}C - \Delta^{14}C_{nat}$). In calculations using the SiO_2 concentrations measured in samples of the same cruise (unpublished data) and as plotted in Figure S1 in Supporting Information S1, we found that the weak bomb ^{14}C signals ($\Delta^{14}C_{bomb} > 0$‰) have penetrated

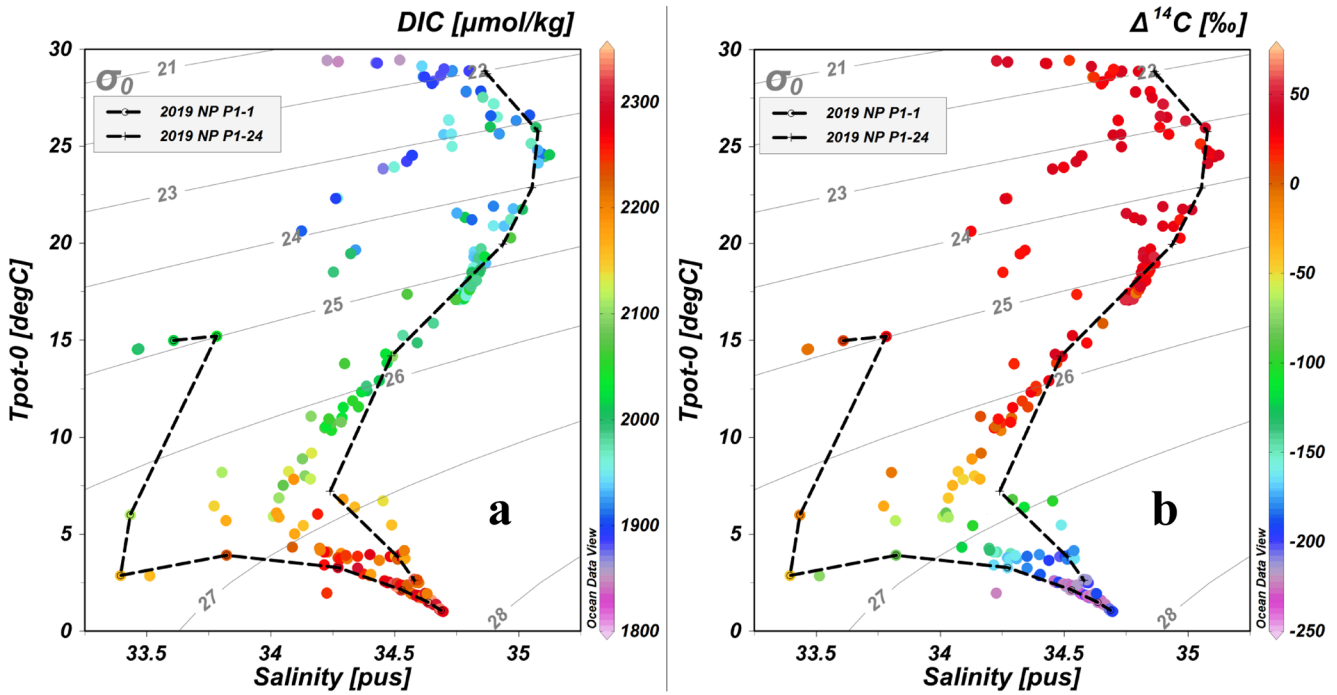

Figure 4. Plots of water temperature versus salinity with (a) concentrations of DIC and (b) Δ^{14}C-DIC values associated with different water masses (represented by different colored points) along the P1 transect in the western NP in November 2019 using ODV.

to very deep depths (>3,000 m) at some stations (25°–35°N) in the NP; this is much deeper than the depth of 1500 m determined in previous studies (Kaizer et al., 2020; Key et al., 2002; Kumamoto et al., 2013).

The Δ^{14}C and $\Delta^{14}C_{bomb}$ values obtained in our study imply that the penetration depth of strong bomb ^{14}C signals varies at different stations (Figure 3d; Figure S1 in Supporting Information S1); this demonstrates that the turnover time of the thermocline circulation in the northwestern subtropical region is latitudinally different. The modern Δ^{14}C values are observed in the upper 250–300 m for stations between 13° and 25°N, which are likely influenced by the North Equatorial Current. The zero isolines of Δ^{14}C values (0‰) are the deepest, and bomb ^{14}C contents in the water are distributed uniformly to a depth of ~500 m at 25°–35°N (Figure 3d). Notably, the depth of the thermocline at 25°–35°N is also greater than the depths at other stations (Figure 2b). This might be related to the adjacent KE Current that brings subtropical waters containing more radiocarbon to the stations at 30°–35°N; this could influence the upper 500 m (Kaizer et al., 2020). The NP subtropical gyre is characterized by anticyclonic circulation, downwelling, and a thick thermocline. In the core of the NP subtropical gyre, the surface water converges and sinks, causing the thermocline to deepen (Figure 2a), and this may lead to the accumulation of surface water with bomb ^{14}C in the region between 25° and 30°N.

In comparison, between 36° and 40°N, where the Δ^{14}C values are significantly lower than those at the other stations and decrease rapidly with depth, the modern bomb ^{14}C signal is seen only in the upper 45–115 m water depth (Figures 3c and 3d). Vertical values of ^{14}C at stations from 36° to 40°N appear to be influenced by the Oyashio Current (Ding et al., 2018), which carries subarctic NPIW southward in the region near 35°–37°N and 143°E east (Qiu & Chen, 2011; Yasuda et al., 1996). Compared to other stations, stations between 35° and 40°N that are influenced by the KE water mass have denser water ($26 < \sigma_0 < 27$) with high DIC concentrations and low Δ^{14}C values in the upper 500 m (Figures 2c, 2f, 3b and 3d). The KE originates from the east coast of Japan at 140°E and 35°N, where the Kuroshio and Oyashio Currents meet and flow eastward toward the open basin of the NP, influencing the hydrology and chemical properties of the resulting water mass (Tsunogai et al., 1995; Tsurushima et al., 2002). The south-flowing Oyashio Current carries subarctic NPIW southward and is characterized by low salinity (33.9–34.1) and dense (σ_0 26.6–26.9) water (Ding et al., 2018; Qiu & Chen, 2011; Talley, 1993). Subarctic water originating in the northwestern subarctic gyre is also characterized by high DIC concentrations and low Δ^{14}C values (Ding et al., 2018) and influences carbon isotope characteristics in the KE region between 35°N and 40°N.

The subarctic NPIW transports a water mass to the south subtropical gyre (15–20°N), thereby affecting the NP thermocline at depths of 300–1,000 m (Itou et al., 2003; Talley, 1993). Kumamoto et al. (2013) calculated the inventory of bomb ^{14}C in DIC within the Pacific Ocean and indicated a deeper penetration depth at 35°N than at other places along the CLIVAR P10N line in 2005; this suggests that the NPIW has played an important role in the ventilation of thermocline water. The denser water masses ($26 < \sigma_0 < 27$) at ~300 to 1,000 m depth between 13° and 40°N at our sampling stations likely originated from the subarctic gyre, which circulates with the NPIW and has low temperature and salinity values (Figure 2).

4.2. Low $\Delta^{14}C$-DIC Values in Pacific Deep Water

A minimum in $\Delta^{14}C$ values (−207‰ to −243‰) occurs in the Pacific Deep Water (PDW) between 2,000 and 3,000 m along the P1 section in the western NP (Figures 3c and 3d). Similar $\Delta^{14}C$ distribution trends in the NP have been reported in other studies, showing that the average $\Delta^{14}C$ values in the PDW are significantly lower than those above and below the PDW layer (Druffel et al., 2008; Masiello et al., 1998; Shan et al., 2020) and reflecting a longer cycle time scale for this water mass. These patterns in the NP have been explained by the observation that the southward return flow of PDW decreases the $\Delta^{14}C$ values of DIC because the PDW has been isolated from the atmosphere longer than has the Pacific bottom water (PBW; Masiello et al., 1998). A clear low $\Delta^{14}C$ layer at this depth (2,000–3,000 m, Figure 3d) indicates that a downward trend from north to south is present in the $\Delta^{14}C$ signature in the western NP deep water. Druffel et al. (2019) observed that $\Delta^{14}C$ values increase at more southern latitudes in the PDW of the central Pacific, opposite to the expectation as the PDW water mass travels southward, and the reverse aging was attributed to mixing of water from above and below the PDW (Druffel et al., 2019). As illustrated in Figure 5a, plots of DIC $\Delta^{14}C$ values as a function of latitude for samples in the PDW obtained on different cruises (line P1 in 2019, line P10N in 2005, line P10 in 1993, and line P16N in 2015) show some differences. The $\Delta^{14}C$ values for our samples obtained between 2,000 and 3,500 m depth decrease slightly with latitude in a southward direction, yielding the expected result. However, this expected trend could also be due to the uncertainty of our measurements (±3–4‰). For all of the cruises, a lack of consistency with the expected results could be explained by shifts in deep water circulation (Druffel et al., 2008; Roussenov et al., 2004). Roussenov et al. (2004) used a one-and-a-half-layer model for deep water and an isopycnal circulation model to show that $\Delta^{14}C$ values in the deep Pacific were controlled by the rapid horizontal transport of young $\Delta^{14}C$ in bottom water from the south with a much slower balance between advection diffusion and decay of ^{14}C in the vertical direction. Increasing diapycnal mixing could lead to a greater northward penetration of bottom water with a younger ^{14}C age in the northern part of the NP and vice versa, indicating that the horizontal transport of bottom waters varies on a centennial time scale. As discussed in the preceding section, bomb ^{14}C was slightly mixed to 2500 m in the western NP subtropical ocean in our study; this could be one reason for the high $\Delta^{14}C$ value at ~35°N.

Studies have demonstrated that the distribution of DIC $\Delta^{14}C$ in the open ocean can be predicted by the solution mixing model and that DIC can be used as a relatively conservative tracer of the movement of water masses and the homogenization of water parcels (Beaupre & Aluwihare, 2010; Ding et al., 2020; Druffel et al., 2019). In the Keeling plots in Figure 6a, there is a good correlation between $\Delta^{14}C$ and $[DIC]^{-1}$ ($r^2 = 0.78$, $p < 0.001$) for samples below 500 m (and of the average values for samples above 500 m) in our study. The slope (4.21×10^6) and intercept (−2,055) values of the Keeling plot for samples below 500 m are comparable to the values for the KE region reported in previous studies (4.0×10^6, −2026, Ding et al., 2018) and to those for the Southern Ocean (5.64×10^6, −2670), the eastern NP (4.29×10^6, −2040) and the central NP (5.28×10^6, −2470) reported by Beaupre and Aluwihare (2010). These plots again illustrate that DIC in the deep ocean (although not in the upper water layer at 0–500 m) is a relatively conservative tracer and that its distribution and isotopic signatures are influenced mainly by the processes of water mass movement and mixing. As shown in Figure 6b, the NP deep water (1,500–3,000 m) is characterized by the highest DIC concentrations and lowest $\Delta^{14}C$ values, illustrating that the PDW comes mainly from the upwelling of AABW and that the influence of water above the PDW should be slight (Figure 6b). An increase in $\Delta^{14}C$ values of up to 20‰ over the 14-year period between 2005 and 2019 is observed on comparison of the values obtained at 2,500 m depth at 36°N of the P1 line in 2019 (−216‰) with those obtained at the 35°N 10N line near our NP station in 2005 (~236‰; Figure 5a; Tables S1 and S2 in Supporting Information S1). The bomb signal above PDW may be too weak to cause such an increase (20‰) in $\Delta^{14}C$. Therefore, we believe that the variability in the $\Delta^{14}C$ values with time represents changes in circulation and mixing in PDW masses that caused shifts in the baseline $\Delta^{14}C$ signature.

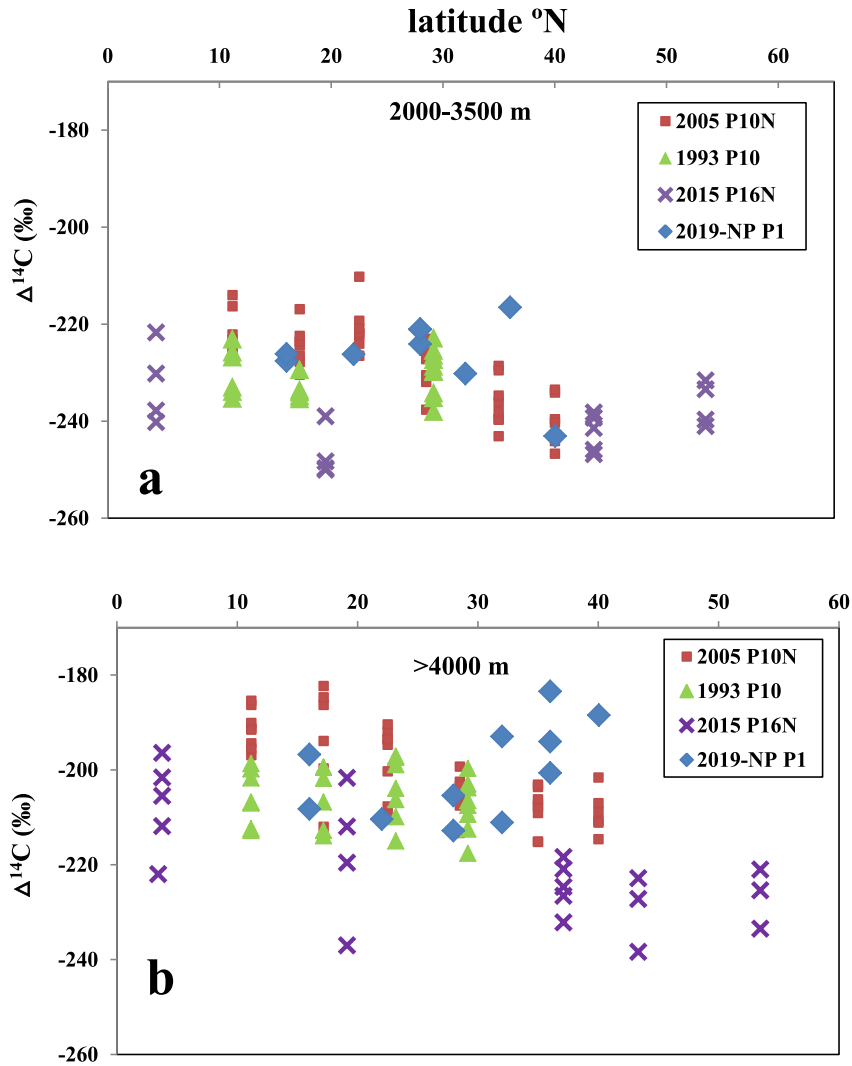

Figure 5. Comparison plots of Δ^{14}C-DIC values as a function of latitude for samples from different cruises (line P1 in 2019, line P10N in 2005, line P10 in 1993, and line P16N in 2015). (a) Between depths of 2,000 and 3,500 m and (b) below 4,000 m (Pacific Bottom Water, PBW).

Most data points for samples in the upper 500 m fell into an almost horizontal line and were positioned below the fitting line (Figure 6a). This is attributed to the strong influence of air-sea exchange and upper layer water mixing. In our previous study, however, the Keeling plot for the six deep stations in the KE region (29°–37°N) showed high coefficients ($r^2 = 0.84$) for all samples collected in May, including samples from the surface waters (Ding et al., 2018). These seasonal variations indicate the strong influence of biological processes on DIC in the euphotic zone. High primary production in the KE region in May reduced the concentration of DIC by 10%–15% (Ding et al., 2018) compared with the values observed in November. In winter, strong winds could mix the upper water and result in a homogeneous distribution of atmospheric ^{14}C signals in the upper 500 m depth at most stations (Figures 3c, 3d and 6a).

4.3. Elevated ^{14}C-DIC in Bottom Water of the Western NP

The deep circulation of the world ocean plays a central role in the carbon cycle. Similar to previous reports, our study finds that DIC concentrations increase along with deep ocean circulation (Figures 3a and 3b) and that the majority of DIC is thus located in the deep ocean, making the Pacific Ocean the most important carbon reservoir (Key et al., 2004; Marinov & Sarmiento, 2004). The deepest part of the global overturning circulation is

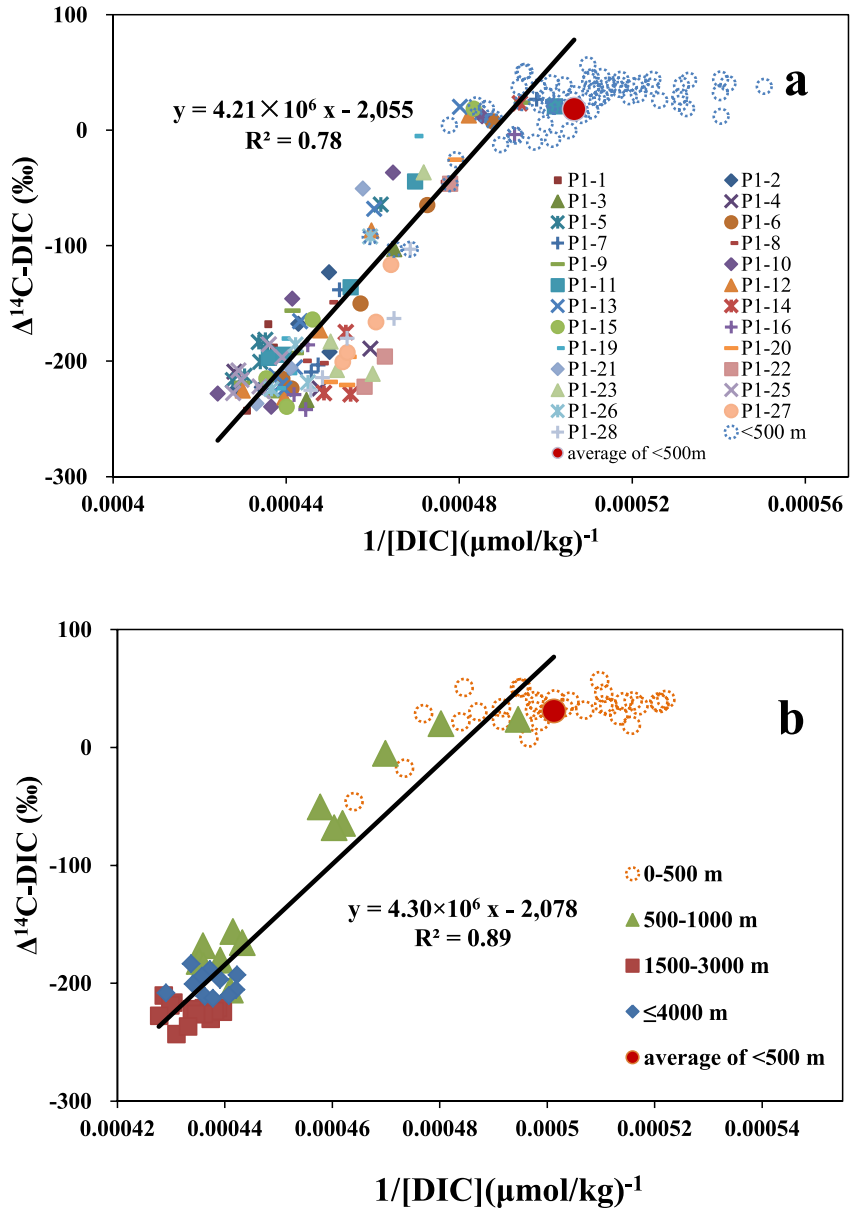

Figure 6. Keeling plots of Δ^{14}C-DIC versus [DIC] $^{-1}$ measured for (a) water samples at all stations and (b) water samples obtained at the seven whole water depth stations in the western NP in November 2019. The black solid lines are linear regression lines fitted to data points below 500 m and to the average values for water samples in the upper 500 m.

AABW, which forms in the Southern Ocean and flows northward via deep thermohaline circulation (Lavergne et al., 2017; Roussenov et al., 2004). As shown in Figure 5b, plots of the Δ^{14}C-DIC values as a function of latitude for samples collected during the different cruises (line P1 in 2019, line P10N in 2005, line P10 in 1993, and line P16N in 2015) below 4,000 m (PBW) display some large variations. The P16N values show a significant correlation with latitude in the central NP (150°W) that decreases as latitude increases (Druffel et al., 2019). In general, the values reported for the P16N line in 2015 are lower than those for the P10N (2005) and P10 (1993) lines. In comparison, the Δ^{14}C values that we measured in deep water during the 2019 cruise do not show a decreasing pattern with latitude (Figure 5b). These differences could indicate that temporal and spatial variabilities in Δ^{14}C exist in the deep NP. In the region of 30°–40°N, the Δ^{14}C values along the P1 line in 2019 are obviously higher than those measured during the other cruises. As discussed in Section 4.2, changes in deep water circulation patterns offer a plausible explanation of the variabilities in Δ^{14}C. The presence of a high-speed current would likely vary the physical properties of a water mass at a single site, including the DIC Δ^{14}C signature (Druffel et al., 2008;

Masiello et al., 1998; Roussenov et al., 2004). Low bomb ^{14}C levels might have penetrated the NP Ocean to a depth of ~2,500 m or greater. However, it is difficult to attribute the source of bomb ^{14}C to physical mixing of upper waters with the deep waters of the NP Ocean during the hundreds- to thousands-of-years transit times of deep-water masses (Druffel et al., 2008). The $\Delta^{14}C$ values of particulate organic carbon (POC) in the deep water are modern, and one possible source of bomb ^{14}C would be input of remineralized bomb-laden POC from surface waters by lateral transport and vertical sinking (Druffel et al., 2008; Kim et al., 2017; Shan et al., 2020). However, the potential change of $\Delta^{14}C$ by vertical transport of POC remineralization is too small to significantly change the $\Delta^{14}C$ of DIC (Druffel et al., 2008; Masiello et al., 1998). Horizontal variability is still likely the main reason for the changes in the DIC $\Delta^{14}C$ signature of PDW.

4.4. Decadal Variations in DIC Radiocarbon Along the P1 Transect

A comparison of our $\Delta^{14}C$ values for the P1 transect with previously measured $\Delta^{14}C$-DIC values along nearby transects in the western NP (WOCE line P10 149.331°E, 1993 and CLIVAR line P10N 149.331°E, 2005) shows high similarity as well as noticeable differences (Figure 7). The strong bomb ^{14}C signal in the surface layer (0–500 m) has weakened since 1993, but bomb ^{14}C has clearly penetrated deeper into the upper 2,000 m in the cross-section of the western NP as of 2019 (Figure 7a) compared with 2005 (Figure 7b) and 1993 (Figure 7c). The bomb ^{14}C lost from the upper water of the NP should have been transported into deep water or into other basins (Kumamoto et al., 2013). To quantitatively calculate the decadal changes in bomb ^{14}C in the western NP, we also compared the depth profiles of $\Delta^{14}C$ for eight selected stations from 35° to 13°N sampled during 2019 along the P1 transect with those for nearby stations sampled along CLIVAR line P10N in 2005 and WOCE line P10 in 1993, as shown in Figure 8. Based on the differences, we calculated the decadal changes in the bomb inventory in surface waters. The surface ^{14}C-DIC values in our samples are approximately 60–110‰ lower than those observed at nearby stations along the P10 section in 1993 and approximately 26–80‰ lower than those observed along the P10N section in 2005 (Figure 8). The global average $\Delta^{14}C$ value in atmospheric CO_2 decreased from ~150‰ in 1990 to ~50‰ in 2010 (Hua et al., 2013), and the average Northern Hemisphere value decreased to ~30‰ in 2018 (Gao et al., 2019; Zigah et al., 2017). These changes in atmospheric bomb ^{14}C, as well as transport into deeper waters and/or advection away from the region, have decreased the $\Delta^{14}C$ signature of the upper ocean, and this explains the changes in $\Delta^{14}C$ in surface water observed over the last three decades (Kumamoto et al., 2013). The temporal changes in radiocarbon show that the $\Delta^{14}C$ content of surface seawater decreased steadily at a rate of 2.4–2.8‰ yr^{-1} from 1993 to 2005 and that it accelerated at a rate of 2.1–7.0‰ yr^{-1} from 2005 to 2019. We find that the rate of decrease in $\Delta^{14}C$-DIC from 2005 to 2019 was not the same at different latitudes; the fastest rates (5.4–7.0‰ yr^{-1}) occurred at 25°–32°N, and the lowest rates (2.1–2.8‰ yr^{-1}) occurred at 13°–16°N. Kaizer et al. (2020) compared the $\Delta^{14}C$ values of surface water collected from cruises (line P10) in 1993, 2005, and 2012 and found a rapidly decreasing rate from 2005 (3.7–4.0‰ yr^{-1}). The different rates of ^{14}C decrease in surface water cannot be fully explained by different rates of air-sea exchange in different areas. The downwelling of bomb ^{14}C and its transport along isopycnal layers probably have more significant impacts on the dilution of ^{14}C (Kaizer, et al., 2020). The uptake rates of anthropogenic CO_2 in the 1990s and the 2000s in the Pacific Ocean reveal that the values of anthropogenic CO_2 storage were <0.7 μmol kg^{-1} along the P10 section (Kouketsu et al., 2013); an increase in DIC by 1 μmol kg^{-1} of pure fossil carbon would lower the $\Delta^{14}C$-DIC values by only ~0.5‰. These results indicate that active isopycnal mixing in the study area and downwelling of the water mass have accelerated the diffusion of bomb-produced ^{14}C in the NP subtropical gyre to rates of 5.4–7.0‰ yr^{-1}.

A comparison of the ^{14}C profiles at depths of 0–2,000 m over the three decades also indicates that the largest changes occurred in the upper 1,000 m among the stations (Figure 8). Bomb ^{14}C enters the intermediate water by mixing with the upper water. In the upper NPIW, we find a definite decreasing trend with time in the temporal variations in $\Delta^{14}C$. In the middle and lower layers of the NPIW, this decrease with time is less obvious from north (29°N) to south (13°N), and the 1993 values are even the most depleted at the southernmost stations (16°N, 13°N, Figure 8g and 8h). The vertical inventory of bomb ^{14}C has been reported to decline significantly in the northwestern subtropical region (Kumamoto et al., 2013). The results of a study that modeled bomb ^{14}C in the Pacific Ocean support the interpretation that bomb ^{14}C is transported from the Pacific to the Indian Ocean along the Indonesian Throughflow (Rodgers et al., 2000). Another likely factor is that bomb ^{14}C is transported southward to the southwestern NP and that its level increases in the intermediate water at the southern stations (Kaizer et al., 2020; Povinec et al., 2004). The bomb ^{14}C peak likely penetrated the ocean interior gradually. Therefore, the decreasing trend and the small change in ^{14}C in the middle and lower layers of the NPIW in the

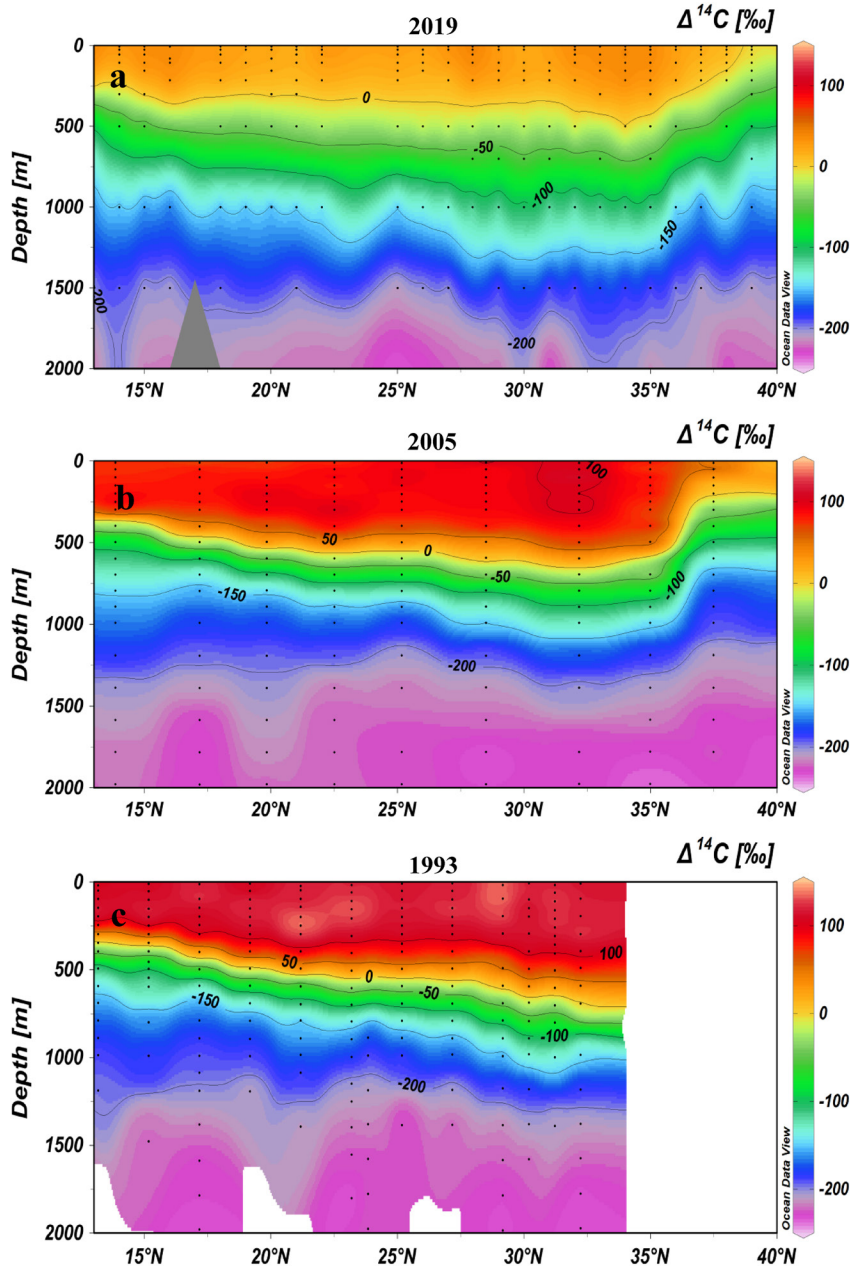

Figure 7. Latitudinal distributions of the Δ^{14}C-DIC values measured for (a) transect P1 in 2019 in our study; (b) CLIVAR line P10N in 2005; and (c) WOCE line P10 in 1993 in the upper 2,000 m of water in the northwestern NP using ODV. The data for lines P10N and P10 were obtained from the GLODAP database (https://www.glodap.info/) and are shown in Tables S2 and S3 in Supporting Information S1.

northern region from the 1990s to the early 2000s and thence to 2019 (Figures 8a–8e, 22°–35°N) indicates that the bomb ^{14}C peak reached that area prior to the 1990s. On the other hand, the ^{14}C values in the middle and lower NPIW of the southern region increased between the 1990s and the 2000s and decreased between the 2000s and 2019 (Figure 8h), implying that the bomb ^{14}C peak passed through this area between the 1990s and the 2000s or between the 1990s and 2019.

We also compare our Δ^{14}C values at three stations (P1-13, P1-19, and P1-25) with those in profiles obtained during WOCE in 1993 (Key et al., 2002) and CLIVAR in 2005 (Kumamoto et al., 2013) for depths between 1,000 and 6,000 m. As shown in Figure 9, at stations located between ~28° and 29°N (Figure 9a), the 2019 Δ^{14}C values

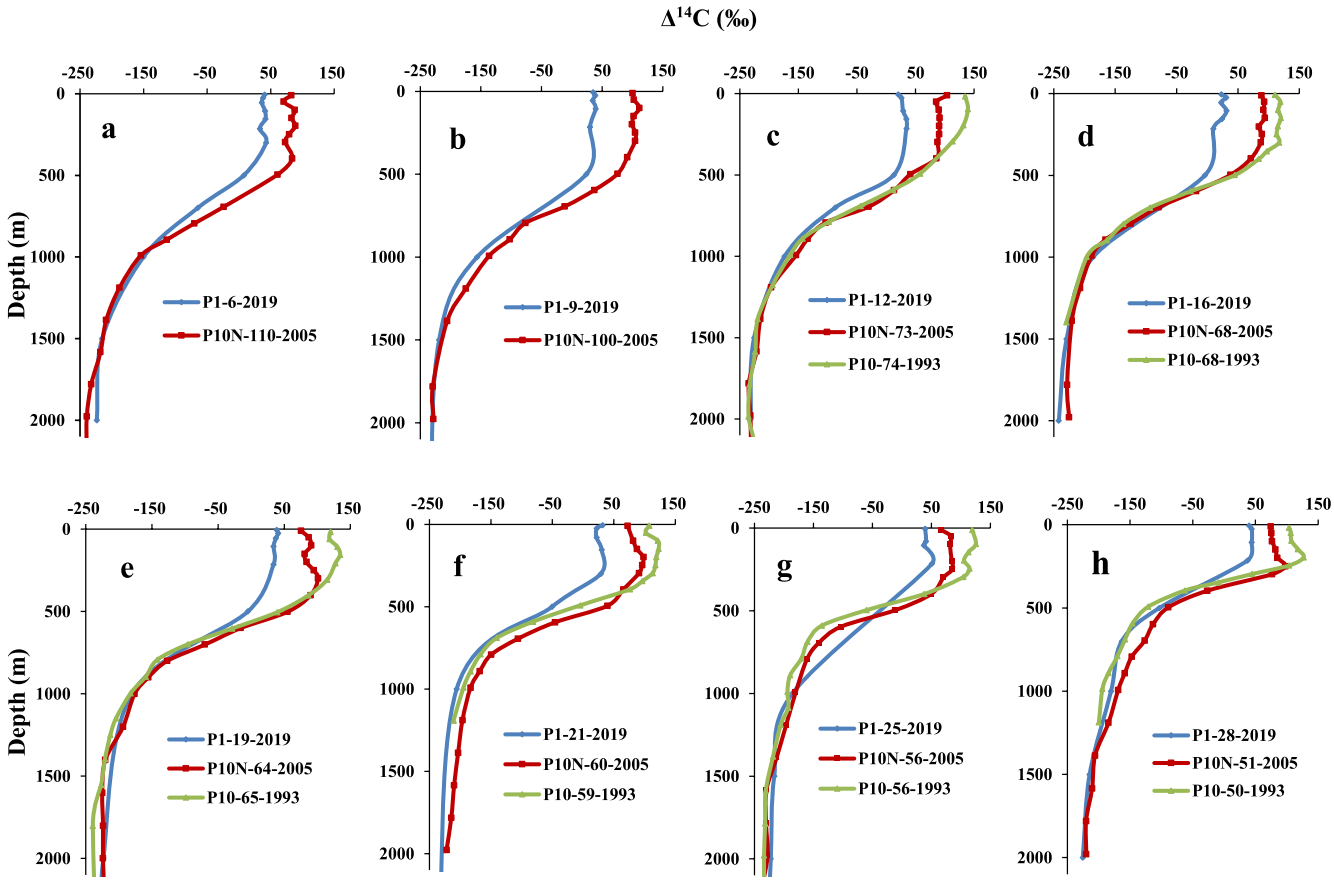

Figure 8. Comparison of the depth profiles of the Δ^{14}C-DIC values measured for stations along transect P1 in 2019 in our study with those obtained at nearby stations along CLIVAR line P10N in 2005 and WOCE line P10 in 1993 in the upper 2,000 m of water in the northwestern NP. The data for lines P10N and P10 are from the GLODAP database (https://www.glodap.info/) and are shown in Tables S2 and S3 in Supporting Information S1. The stations from (a) to (h) are distributed from north (~35°N) to south (~13°N). See Figure S2 in Supporting Information S1 for the locations of these stations.

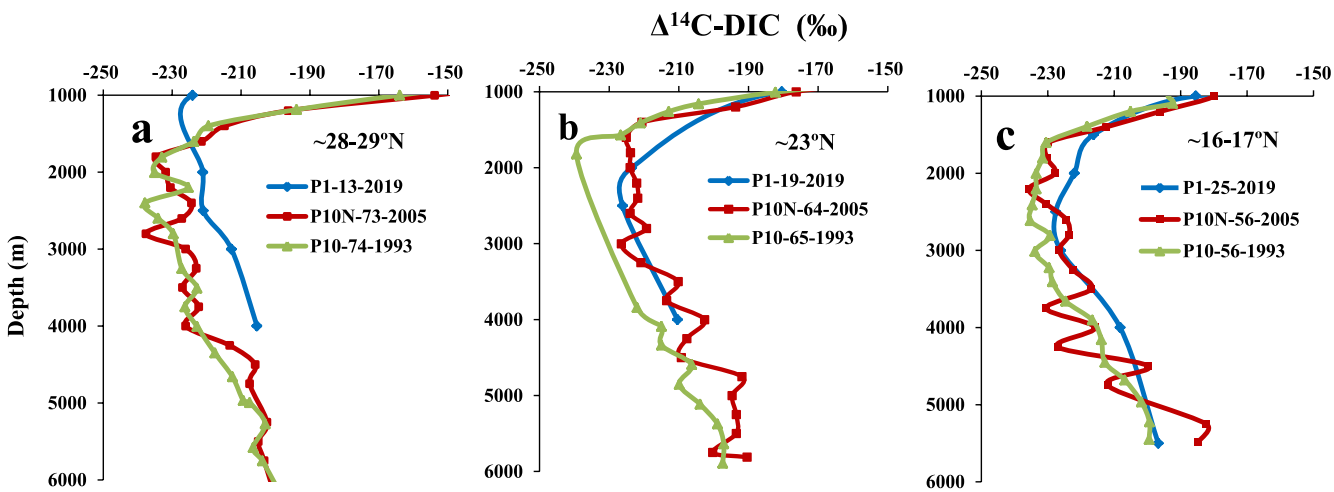

Figure 9. Depth profiles of the Δ^{14}C-DIC values measured for three stations along transect P1 in 2019 in our study (Sta P1-13, 28°N, 150°E; Sta P1-19, 22°N, 150°E; and Sta P1-25, 16°N, 150°E) and profiles obtained during WOCE in 1993 (Sta P10-74, 29.1°N, 149.3°E; Sta P10-65, 22.5°N, 149.3°E; and Sta P10-56, 17.2°N, 149.3°E) and during CLIVAR in 2005 (Sta P10N-73, 28.5°N, 149.3°E; Sta P10N-64, 23.2°N, 149.3°E; and Sta P10N-56, 17.2°N, 149.3°E) at water depths of 1,000–6,000 m in the western NP (GLODAP database: https://www.glodap.info/). See Figure S3 in Supporting Information S1 for the locations of these stations.

are higher than the values for similar depths at the previous cruise stations. The $\Delta^{14}C$ values measured in 2019 are comparable to those measured in 2005, and both are higher than the 1993 values for water below 1,500 m depth at ~23°N (Figure 9b). The vertical profiles of $\Delta^{14}C$ at the southern stations (~16°–17°N) also show higher values in 2019 than in 1993 (Figure 9c), but the values obtained in 2005 fluctuated greatly with depth. At the same time, the depth at which the minimum $\Delta^{14}C$ value occurred appears to have varied with time (Figure 9). Temporal changes in $\Delta^{14}C$ in the western NP deep waters have been observed over the last three decades. We expect that changes in the isopycnal circulation and in advection diffusion in deep waters will cause shifts in the baseline $\Delta^{14}C$ signature, as suggested by Druffel et al. (2008). In comparison, however, the changes in $\Delta^{14}C$ in deep water (>2,000 m) are less pronounced than those that have occurred in the upper 500 m water depth in the NP in the last three decades.

5. Conclusions

The results for radiocarbon in DIC measured along the P1 transect in the western NP reveal that the movement of different water masses and the penetration of anthropogenic CO_2 through air-sea mixing in the ocean influence the distribution of DIC and its isotopic signatures in the western NP Ocean. The profiles and latitudinal distributions of DIC concentrations and $\Delta^{14}C$ display obvious gradient changes in the vertical direction. High $\Delta^{14}C$ values in surface waters show that strong bomb $\Delta^{14}C$ signals mix and diffuse into the upper 200–500 m through air-sea exchange and isopycnal mixing. The "old" NPIW transports a water mass from the subarctic gyre that carries low-$\Delta^{14}C$ water to the subtropical gyre, affecting the $\Delta^{14}C$ values of NP thermocline water at depths of 300–1,000 m from 36° to 40°N. Increased diapycnal mixing could lead to greater northward penetration of bottom water with relatively young $\Delta^{14}C$ ages into the northern NP Ocean and cause the $\Delta^{14}C$ values in water below 4,000 m at 28°–40°N to decrease with increasing latitude; such changes would be opposite in character to those influenced by the deep thermohaline circulation. There are minimum $\Delta^{14}C$ values in the NP deep water that are explained by the decreasing $\Delta^{14}C$ values of the DIC caused by the southward return flow of Pacific deep water.

The abundance of $\Delta^{14}C$ in DIC in the upper water layers along the P1 transect in the NP decreased significantly in 2019 compared with the values recorded in 1993 and 2005. These decadal changes reflect the decrease in bomb ^{14}C in DIC in surface waters since the early 1990s. Faster rates of decrease in $\Delta^{14}C$ values in surface waters are found for 2005–2019 (2.1–7.0‰ yr^{-1}) than for 1993–2005 (2.4–2.8‰ yr^{-1}). The downwelling of the water mass might accelerate the diffusion of bomb ^{14}C in the NP subtropical gyre (25°–32°N), with the fastest rates of decrease (5.4–7.0‰ yr^{-1}) having occurred between 25° and 32°N from 2005 to 2019. The different decadal changes in ^{14}C in the NPIW from north to south prove that bomb ^{14}C is transported southward to the southwestern NP. One of the likely pathways for this transport is that bomb ^{14}C is transported from the Pacific into the Indian Ocean via the Indonesian Throughflow. Changes in the diapycnal circulation and advection diffusion in deep waters might have resulted in shifts in the baseline $\Delta^{14}C$ signature.

Conflict of Interest

The authors declare no conflicts of interest relevant to this study.

Data Availability Statement

All the data used in this paper are presented in Table S1 in Supporting Information S1 and are publicly available at figshare.com (via https://doi.org/10.6084/m9.figshare.17789714.v3).

Acknowledgments
The authors would like to thank the captain and crew of *R/V* Dongfanghong-3 for assistance during the cruise. The authors thank the staff at the Center for Isotope Geochemistry and Geochronology (CIGG) for measuring the ^{13}C and ^{14}C values of the samples. Financial support for this work was provided by the National Natural Science Foundation of China (Grants # 91858210, 41776082, and 41476057) and the Western Pacific P1 Section Observation Voyage of the Shandong Major Science and Technology Innovation Project (2018SDKJ0105-1).

References

Bauer, J. E., Williams, P. M., & Druffel, E. R. M. (1992). ^{14}C activity of dissolved organic carbon fractions in the north central Pacific and Sargasso Sea. *Nature*, *357*, 667–670. https://doi.org/10.1038/357667a0

Beaupre, S. R., & Aluwihare, L. (2010). Constraining the 2-component model of marine dissolved organic radiocarbon. *Deep Sea Research Part II: Topical Studies in Oceanography*, *57*, 1494–1503. https://doi.org/10.1016/j.dsr2.2010.02.017

Bien, G. S., Rakestraw, N. W., & Suess, H. E. (1963). Radiocarbon concentration in Pacific Ocean water. *Tellus*, *12*(4), 436–443. https://doi.org/10.1111/j.2153-3490.1960.tb01330.x

Broecker, W. S., Olson, E. A., & Orr, P. C. (1960). Radiocarbon measurements and annual rings in cave formations. *Nature*, *185*(4706), 93–94. https://doi.org/10.1038/185093a0

Broecker, W. S., Peteet, D. M., & Rind, D. (1985). Does the ocean–atmosphere system have more than one stable mode of operation? *Nature*, *315*(6014), 21–26. https://doi.org/10.1038/315021a0

Broecker, W. S., Sutherland, S., Smethie, W., Peng, T. H., & Ostlund, G. (1995). Oceanic radiocarbon: Separation of the natural and bomb components. *Global Biogeochemical Cycles*, *9*(2), 263–288. https://doi.org/10.1029/95GB00208

Ding, L., Ge, T., Gao, H., Luo, C., Xue, Y., Druffel, E. R. M., & Wang, X. (2018). Large variability of dissolved inorganic radiocarbon in the Kuroshio Extension of the northwest North Pacific. *Radiocarbon*, *60*(2), 691–704. https://doi.org/10.1017/RDC.2017.143

Ding, L., Qi, Y., Shan, S., Ge, T., Luo, C., & Wang, X. (2020). Radiocarbon in dissolved organic and inorganic carbon of the South China Sea. *Journal of Geophysical Research: Oceans*, *125*(4). https://doi.org/10.1029/2020JC016073

Druffel, E. R. M., Bauer, J. E., Griffin, S., Beaupré, S. R., & Hwang, J. (2008). Dissolved inorganic radiocarbon in the north Pacific Ocean and Sargasso Sea. *Deep Sea Research Part I: Oceanographic Research Papers*, *55*(4), 451–459. https://doi.org/10.1016/j.dsr.2007.12.007

Druffel, E. R. M., Griffin, S., Wang, N., Garcia, N. G., McNichol, A. P., Key, R. M., & Walker, B. D. (2019). Dissolved organic radiocarbon in the Central Pacific Ocean. *Geophysical Research Letters*, *46*(10), 5396–5403. https://doi.org/10.1029/2019GL083149

Druffel, E. R. M., Williams, P. M., Bauer, J. E., & Ertel, J. R. (1992). Cycling of dissolved and particulate organic matter in the open ocean. *Journal of Geophysical Research*, *97*(C10), 15639–15659. https://doi.org/10.1029/92JC01511

Gao, P., Zhou, L., Liu, K., & Xu, X. (2019). Radiocarbon in the maritime air and sea surface water of the South China Sea. *Radiocarbon*, *61*(2), 461–472. https://doi.org/10.1017/RDC.2018.100

Ge, T., Wang, X., Zhang, J., Luo, C., & Xue, Y. (2016). Dissolved inorganic radiocarbon in the Northwest Pacific continental margin. *Radiocarbon*, *58*(3), 517–529. https://doi.org/10.1017/RDC.2016.23

Gruber, N. (2011). Warming up, turning sour, losing breath: Ocean biogeochemistry under global change. *Philosophical Transactions of the Royal Society A: Mathematical, Physical and Engineering Sciences*, *369*, 1980–1996. https://doi.org/10.1098/rsta.2011.0003

Gruber, N., Gloor, M., Fletcher, S. E., Doney, S. C., Dutkiewicz, S., Follows, M. J., et al. (2009). Oceanic sources, sinks, and transport of atmospheric CO_2. *Global Biogeochemical Cycle*, *23*, GB1005. https://doi.org/10.1029/2008GB003349

Hu, D., Wu, L., Cai, W., Gupta, A. S., Ganachaud, A., Qiu, B., et al. (2015). Pacific western boundary currents and their roles in climate. *Nature*, *522*(7556), 299–308. https://doi.org/10.1038/nature14504

Hua, Q., Barbetti, M., & Rakowski, A. Z. (2013). Atmospheric radiocarbon for the period 1950–2010. *Radiocarbon*, *55*(4), 2059–2072. https://doi.org/10.2458/azu_js_rc.v55i2.16177

Itou, M., Ono, T., & Noriki, S. (2003). Provenance of intermediate waters in the western north pacific deduced from thermodynamic imprint on $\delta^{13}C$ of DIC. *Journal of Geophysical Research*, *108*(C11), 3347. https://doi.org/10.1029/2002JC001746

Kaizer, J., Kumamoto, Y., Molnár, M., Palcsu, L., & Povinec, P. P. (2020). Temporal changes in tritium and radiocarbon concentrations in the western North Pacific Ocean (1993–2012). *Journal of Environmental Radioactivity*, *218*, 106238. https://doi.org/10.1016/j.jenvrad.2020.106238

Key, R. M. (1996). WOCE Pacific Ocean radiocarbon program. *Radiocarbon*, *38*(3), 415–423. https://doi.org/10.1017/S003382220003006X

Key, R. M., Kozyr, A., Sabine, C. L., Lee, K., Wanninkhof, R., Bullister, J. L., et al. (2004). A global ocean carbon climatology: Results from Global Data Analysis Project (GLODAP). *Global Biogeochemical Cycles*, *18*, GB4031. https://doi.org/10.1029/2004GB002247

Key, R. M., Quay, P. D., Jones, G. A., McNichol, A. P., Von Reden, K. F., & Schneider, R. J. (1996). WOCE AMS Radiocarbon I: Pacific Ocean results (P6, P16 and P17). *Radiocarbon*, *38*(3), 425–518. https://doi.org/10.1017/S0033822200030071

Key, R. M., Quay, P. D., Schlosser, P., McNichol, A. P., von Reden, K. F., Schneider, R. J., et al. (2002). WOCE Radiocarbon IV: Pacific Ocean results; P10, P13N, P14C, P18, P19 & S4P. *Radiocarbon*, *44*(1), 239–392. https://doi.org/10.1017/S0033822200064845

Kim, M., HwangRho, J. T., Lee, T., Lee, T., Kang, D.-J., Chang, K.-I., et al. (2017). Biogeochemical properties of sinking particles in the southwestern part of the East Sea (Japan Sea). *Journal of Marine Systems*, *167*, 33–42. https://doi.org/10.1016/j.jmarsys.2016.11.001

Kouketsu, S., Murata, A., & Doi, T. (2013). Decadal changes in dissolved inorganic carbon in the Pacific Ocean. *Global Biogeochemical Cycles*, *27*(1), 65–76. https://doi.org/10.1029/2012GB004413

Kumamoto, Y., Murata, A., Kawano, T., Watanabe, S., & Fukasawa, M. (2013). Decadal changes in bomb-produced radiocarbon in the Pacific Ocean from the 1990s to 2000s. *Radiocarbon*, *55*(2–3), 1641–1650. https://doi.org/10.2458/azu_js_rc.55.16238

Kumamoto, Y., Murata, A., Saito, C., Honda, M., & Kusakabe, M. (2002). Bomb radiocarbon invasion into the northwestern North Pacific. *Deep Sea Research Part II: Topical Studies in Oceanography*, *49*(24–25), 5339–5351. https://doi.org/10.1016/S0967-0645(02)00194-7

Lavergne, C. D., Madec, G., Roquet, F., Holmes, R. M., & Mcdougall, T. J. (2017). Abyssal ocean overturning shaped by seafloor distribution. *Nature*, *551*(7679), 181–186. https://doi.org/10.1038/nature24472

Lemke, P., Ren, J., Alley, R. B., Alison, I., Carrasco, J., Flato, G., et al. (2007). Climate change 2007: The physical science basis. Contribution of working group I to the fourth assessment report of the intergovernmental panel on climate change. In S. Solomon, D. Qin, M. Manning, Z. Chen, M. Marquis, K. B. Averyt et al. (Eds.), *Technical summary* (pp. 339–378). Cambridge University Press.

Ma, X., Jing, Z., Chang, P., Liu, X., Montuoro, R., Justin, S. R., et al. (2016). Western boundary currents regulated by interaction between ocean eddies and the atmosphere. *Nature*, *535*(7613), 53–537. https://doi.org/10.1038/nature18640

Macdonald, A. M., Mecking, S., Robbins, P. E., Toole, J. M., Johnson, G. C., Talley, L., et al. (2009). The WOCE-era 3-D Pacific Ocean circulation and heat budget. *Progress in Oceanography*, *82*(4), 281–325. https://doi.org/10.1016/j.pocean.2009.08.002

Marinov, I., & Sarmiento, J. L. (2004). The role of the oceans in the global carbon cycle: An overview. In M. Follows, & T. Oguz, (Eds.), *The ocean carbon cycle and climate* (pp. 251–295). Springer. https://doi.org/10.1007/978-1-4020-2087-2_8

Masiello, C. A., Druffel, E. R. M., & Bauer, J. E. (1998). Physical control on dissolved inorganic radiocarbon variability in the California Current. *Deep Sea Research Part II: Topical Studies in Oceanography*, *45*, 617–642. https://doi.org/10.1016/S0967-0645(97)00096-9

McNichol, A. P., & Jones, G. A. (1991). Measuring ^{14}C in seawater ΣCO_2 by accelerator mass spectrometry. In T. Joyce, C. Corry, & M. Stalcup, (Eds.), *World ocean circulation experiment operations manual* (pp. >71). WHPO Publication.

McNichol, A. P., Jones, G. A., Hutton, D. L., Gagnon, A. R., & Key, R. M. (1994). The rapid preparation of seawater ΣCO_2 for radiocarbon analysis at the National Ocean Sciences AMS Facility. *Radiocarbon*, *36*(2), 237–246. https://doi.org/10.1017/S0033822200040522

McNichol, A. P., Schneider, R. J., von Reden, K. F., Gagnon, A. R., Elder, K. L., Nosams, K., et al. (2000). Ten years after—The WOCE AMS radiocarbon program. *Nuclear Instruments and Methods in Physics Research Section B: Beam Interactions with Materials and Atoms*, *172*(1–4), 479–484. https://doi.org/10.1016/S0168-583X(00)00093-8

Povinec, P. P., Aramaki, T., Burr, G. S., Timothy Jull, A. J., Liong Wee Kwong, L., & Togawa, O. (2004). Radiocarbon in the water column of the southwestern North Pacific Ocean—24 years after GEOSECS. *Radiocarbon*, *46*(2), 583–594. https://doi.org/10.1017/S0033822200035621

Qiu, B. O., & Chen, S. (2011). Effect of decadal Kuroshio extension jet and eddy variability on the modification of north pacific intermediate water. *Journal of Physical Oceanography*, *41*(3), 503–515. https://doi.org/10.1175/2010JPO4575.1

Rodgers, K. B., Schrag, D. P., Cane, M. A., & Naik, N. H. (2000). The bomb ^{14}C transient in the Pacific Ocean. *Journal of Geophysical Research: Oceans*, *105*(C4), 8489–5412. https://doi.org/10.1029/1999JC900228

Rogachev, K. A., Carmack, E. C., & Salomatin, A. S. (2000). Recent thermohaline transition in the Pacific western subarctic boundary currents and their fresh core eddies: The response of sound-scattering layers. *Journal of Marine Systems*, *26*(3), 239–258. https://doi.org/10.1016/S0924-7963(00)00036-1

Roussenov, V., Williams, R. G., Follows, M. J., & Key, R. M. (2004). Role of bottom water transport and diapycnic mixing in determining the radiocarbon distribution in the Pacific. *Journal of Geophysical Research*, *109*, C06015. https://doi.org/10.1029/2003JC002188

Sarnthein, M., Schneider, B., & Grootes, P. M. (2013). Peak glacial ^{14}C ventilation ages suggest major draw-down of carbon into the abyssal ocean. *Climate of the Past*, *9*(6), 2595–2614. https://doi.org/10.5194/cp-9-2595-2013

Schlitzer, R. (2015). *Ocean data view*. Retrieved from http://odv.awi.de

Schuur, E. A. G., Carbone, M. S., Pries, C. E. H., Hopkins, F. M., & Natali, S. M. (2016). Radiocarbon in terrestrial systems. In E. A. G. Schuur, E. Druffel, & S. E. Trumbore, (Eds.), *Radiocarbon and climate change* (pp. 167–220). Springer. https://doi.org/10.1007/978-3-319-25643-6_6

Shan, S., Qi, Y., Tian, J., Wang, X., Luo, C., Zhou, C., et al. (2020). Carbon cycling in the deep Mariana trench in the western North Pacific Ocean: Insights from radiocarbon proxy data. *Deep Sea Research Part I: Oceanographic Research Papers*, *164*, 103370. https://doi.org/10.1016/j.dsr.2020.103370

Stuiver, M., Östlund, G., Key, R. M., & Reimer, P. J. (1996). Large-volume WOCE radiocarbon sampling in the Pacific Ocean. *Radiocarbon*, *38*(3), 519–561. https://doi.org/10.1017/S0033822200030083

Stuiver, M., & Polach, H. A. (1977). Discussion reporting of ^{14}C data. *Radiocarbon*, *19*(3), 355–363. https://doi.org/10.1017/S0033822200003672

Stuiver, M., Quay, P. D., & Östlund, H. G. (1983). Abyssal water carbon-14 distribution and the age of the world oceans. *Science*, *219*(4586), 849–851. https://doi.org/10.1126/science.219.4586.849

Takahashi, T., Sutherland, S. C., Sweeney, C., Poisson, A., Metzl, N., Tilbrook, B., et al. (2002). Global sea–air CO_2 flux based on climatological surface ocean pCO_2, and seasonal biological and temperature effects. *Deep Sea Research Part II: Topical Studies in Oceanography*, *49*(9–10), 1601–1622. https://doi.org/10.1016/S0967-0645(02)00003-6

Takahashi, T., Sutherland, S. C., Wanninkhof, R., Sweeney, C., Feely, R., Chipman, D. W., et al. (2009). Climatological mean and decadal change in surface ocean pCO_2, and net sea-air CO_2 flux over the global oceans. *Deep Sea Research Part II: Topical Studies in Oceanography*, *56*(8–10), 554–577. https://doi.org/10.1016/j.dsr2.2008.12.009

Talley, L. D. (1993). Distribution and formation of North Pacific intermediate water. *Journal of Physical Oceanography*, *23*(3), 517–537. https://doi.org/10.1175/1520-0485(1993)023<0517:dafonp>2.0.co;2

Talley, L. D. (2013). Closure of the global overturning circulation through the Indian, Pacific, and Southern oceans: Schematics and transports. *Oceanography*, *26*(1), 80–97. https://doi.org/10.5670/oceanog.2013.07

Talley, L. D., & Lynne, D. (1997). North pacific intermediate water transports in the mixed water region. *Journal of Physical Oceanography*, *27*(8), 1795–1803. https://doi.org/10.1175/1520-0485(1997)027<1795:npiwti>2.0.co;2

Tsunogai, S. (2000). North Pacific water's larger potential sink capacity for absorbing anthropogenic CO_2 and the processes recovering it. In N. Handa, E. Tanoue, & T. Hama, (Eds.), *Dynamics and characterization of marine organic matter* (pp. 533–560). Springer. https://doi.org/10.1007/978-94-017-1319-1_22

Tsunogai, S., Ono, T., & Watanabe, S. (1993). Increase in total carbonate in the western north pacific water and a hypothesis on the missing sink of anthropogenic carbon. *Journal of Oceanography*, *49*(3), 305–315. https://doi.org/10.1007/bf02269568

Tsunogai, S., Watanabe, S., Honda, M., & Aramaki, T. (1995). North pacific intermediate water studied chiefly with radiocarbon. *Journal of Oceanography*, *51*(5), 519–536. https://doi.org/10.1007/BF02270522

Tsurushima, N., Nojiri, Y., Imai, K., & Watanabe, S. (2002). Seasonal variations of carbon dioxide system and nutrients in the surface mixed layer at station knot (44°N, 155°E) in the subarctic western north pacific. *Deep Sea Research: Part II Topical Studies in Oceanography*, *49*(24–25), 5377–5394. https://doi.org/10.1016/S0967-0645(02)00197-2

Valsala, V., Maksyutov, S., Telszewski, M., Nakaoka, S., Nojiri, Y., Ikeda, M., & Murtugudde, R. (2012). Climate impacts on the structures of the north pacific air-sea CO_2 flux variability. *Biogeosciences*, *9*, 477–492. https://doi.org/10.5194/bg-9-477-2012

Wakita, M., Watanabe, S., Murata, A., Tsurushima, N., & Honda, M. (2010). Decadal change of dissolved inorganic carbon in the subarctic western North Pacific Ocean. *Tellus B: Chemical and Physical Meteorology*, *62*(5), 608–620. https://doi.org/10.1111/j.1600-0889.2010.00476.x

Walker, B. D., & Xu, X. (2019). An improved method for the sealed-tube zinc graphitization of microgram carbon samples and ^{14}C AMS measurement. *Nuclear Instruments and Methods in Physics Research Section B: Beam Interactions with Materials and Atoms*, *438*, 58–65. https://doi.org/10.1016/j.nimb.2018.08.004

Williams, P. M., & Druffel, E. R. M. (1987). Radiocarbon in dissolved organic matter in the Central North Pacific Ocean. *Nature*, *330*(6145), 246–248. https://doi.org/10.1038/330246a0

Winn, C. D., Li, Y.-H., Mackenzie, F. T., & Karl, D. M. (1998). Rising surface ocean dissolved inorganic carbon at the Hawaii ocean time-series site. *Marine Chemistry*, *60*(1–2), 33–47. https://doi.org/10.1016/S0304-4203(97)00085-6

Xu, X., Trumbore, S. E., Zheng, S., Southon, J. R., Mcduffee, K. E., Luttgen, M., & Liu, J. C. (2007). Modifying a sealed tube zinc reduction method for preparation of AMS graphite targets: Reducing background and attaining high precision. *Nuclear Instruments and Methods in Physics Research Section B: Beam Interactions with Materials and Atoms*, *259*(1), 320–329. https://doi.org/10.1016/j.nimb.2007.01.175

Yasuda, I. (2004). North Pacific intermediate water: Progress in sage (subarctic gyre experiment) and related projects. *Journal of Oceanography*, *60*(2), 385–395. https://doi.org/10.1023/B:JOCE.0000038344.25081.42

Yasuda, I., Okuda, K., & Shimizu, Y. (1996). Distribution and modification of north pacific intermediate water in the Kuroshio-Oyashio interfrontal zone. *Journal of Physical Oceanography*, *26*(4), 448–465. https://doi.org/10.1175/1520-0485(1996)026<0448:DAMONP>2.0.CO;2

Yasunaka, S., Nojiri, Y., Nakaoka, S. I., Ono, T., Mukai, H., & Usui, N. (2014). North Pacific dissolved inorganic carbon variations related to the Pacific decadal oscillation. *Geophysical Research Letters*, *41*(3), 1005–1011. https://doi.org/10.1002/2013GL058987

Zigah, P. K., McNichol, A. P., Xu, L., Johnson, C., Santinelli, C., Karl, D. M., & Repeta, D. J. (2017). Allochthonous sources and dynamic cycling of ocean dissolved organic carbon revealed by carbon isotopes. *Geophysical Research Letters*, *44*(5), 2407–2415. https://doi.org/10.1002/2016GL071348